

ISSN 0280-5316
ISRN LUTFD2/TFRT--5774--SE

Road-Tire Friction Estimation for AFS Vehicle Control

Andreas Andersson

Department of Automatic Control
Lund University
August 2006

Department of Automatic Control Lund Institute of Technology Box 118 SE-221 00 Lund Sweden		<i>Document name</i> MASTER THESIS	
		<i>Date of issue</i> August 2005	
		<i>Document Number</i> ISRN LUTFD/TFRT--5774--SE	
<i>Authors</i> Andreas Andersson		<i>Supervisor</i> Wolfgang Reinelt and Christian Lundquist at ZF Lenksysteme in Schwäbisch Gmünd, Germany. Tore Hägglund at Automatic Control in Lund, Schweden	
		<i>Sponsoring organization</i>	
<i>Title and subtitle</i> Road-Tire Friction Estimation for AFS Vehicle Control. (Skattning av friktion mellan däck och vägbana för reglering av fordon med aktiv framhjulstyrning)			
<i>Abstract</i> <p>Real time information about the current road surface (friction coefficient) would be of great help for most of the vehicle systems of today. Vehicle stability systems like ABS and ESP would perform considerably better with friction knowledge. Dynamic All Wheel Drive torque distributors would, with friction knowledge, substantially enhance the behavior of the vehicle.</p> <p>In this thesis an enhancement of vehicle dynamic control with Active Front Steering was looked upon. The vehicle dynamic control stabilizes the vehicle with electronic steering interventions at the vehicle's front axle. The thesis goal was to enhance the stabilization algorithm by using knowledge of the road-tire friction coefficient as a system input. Two types of friction estimation algorithms were investigated, implemented and tested in a prototype vehicle. The most promising result gave the approach called slip-slope based friction estimation. The hypothesis is that the friction curve's initial slope contains information about the road-tire friction coefficient. With a parallel running gravel/rough road detector, a distinction between three different friction levels is definitely possible.</p> <p>The second approach was friction estimation with the brush model. The brush model is a physical model for describing the tire forces generated during driving (or braking). The road-tire friction coefficient is explicitly included in the model and that makes it very suitable for different types of parameter estimation algorithms. The estimation result, when feeding the algorithm with "good" (perfectly matching estimation data with low noise levels) data, was very satisfying. But usually are the algorithm input data, during normal driving, not very good. Though, friction estimation using the brush model is an interesting approach for the future. Better sensor signals (less noise) and more work with the algorithm details could probably result in a good and reliable friction estimator.</p>			
<i>Keywords</i> Friction Estimation, Slip-Slope, Brush Model, Active Front Steering, Vehicle Dynamics, Vehicle Dynamic Control.			
<i>Classification system and/or index terms (if any)</i>			
<i>Supplementary bibliographical information</i>			
<i>ISSN and key title</i> 0280-5316			<i>ISBN</i>
<i>Language</i> English	<i>Number of pages</i> 50	<i>Recipient's notes</i>	
<i>Security classification</i>			

Acknowledgments

This master thesis was carried out between January 2006 and June 2006 at ZF Lenksysteme GmbH in Schwäbisch Gmünd, Germany.

First I would like to thank my supervisors Christian Lundquist and Dr. Wolfgang Reinelt for giving me the opportunity to do my master thesis work at their department. It has been a great experience for me and I have seen and learned a lot more than I could ever imagine! Special thanks to Christian for taking your time to answer all my questions, for fruitful discussions and all the hours spent on the test track.

Of course I would also like to thank the rest of the people at the department. You have all been patient and supporting! Thanks to Frank, Ralf, Reinhard, Samuel, Gerd, Hendrik and Thomas.

Special thanks to Anders for interesting apartment discussions, endless good parties and relaxing “Kinotags”!

Finally, I would like to thank my examiner, professor Tore Hägglund at the Department of Automatic Control at Lund University, for helping me establish contact with Dr. Reinelt and for sending me all the scientific papers I wished for.

Älmhult, August 2006

Contents

Abstract	i
Acknowledgments	ii
1 Introduction	1
1.1 The AFS System	1
1.2 Vehicle Dynamic Control	2
1.3 Thesis Goal	4
1.4 Friction Estimation Literature Overview	4
1.5 Thesis Limitations	5
1.6 Thesis Outline	5
1.7 Basic Notation used in the Thesis	6
1.7.1 Abbreviations	6
1.7.2 Variables, Constants and Parameters	6
2 Slip-Slope Based Friction Estimation	8
2.1 Outline and Basics of Slip-Slope Based Friction Estimation	8
2.1.1 Slip-Slope Offset	10
2.1.2 Negative Friction Coefficient	11
2.2 Slip-Slope Estimation	11
2.2.1 Linear Regression Model	12
2.2.2 Kalman Filter Input Calculations	12
2.2.3 The Discrete Optimal Kalman Filter	15
2.2.4 Filtering of Measurement Signals	16
2.3 Algorithm Details and Friction Estimation Results	16
2.3.1 The CUSUM Detector	16
2.3.2 Gravel Detection	18
2.3.3 Estimation Results	20

2.3.4	Calculating the Friction Coefficient while ABS Braking . . .	23
2.3.5	Algorithm Details	23
3	Brush Model Based Friction Estimation	25
3.1	Tire Modeling	25
3.2	The Brush Model	27
3.3	Friction Estimation with the Brush Model	30
4	Conclusions	33
4.1	Slip-Slope Based Friction Estimation	33
4.2	Brush Model Based Friction Estimation	34
4.3	Vehicle Dynamic Control with Friction Estimation	34
	Bibliography	37
A	Derivations	39
A.1	Slip Computation During Cornering	39
A.2	Derivation of the Normal Forces	40

Chapter 1

Introduction

This chapter gives a short introduction to the Active Front Steering system and briefly takes up what can be accomplished with such a steering system. The background and motivation to the thesis is also given.

1.1 The AFS System

ZF Lenksysteme GmbH is a joint venture of Robert Bosch GmbH and ZF Friedrichshafen AG. This has resulted in a company containing expertise knowledge within the field of electrical and mechanical engineering for automotive steering systems. One of ZF Lenksysteme's products is the Active Front Steering system (AFS), which allows driver independent steering intervention at the vehicle's front axle. This is a newly developed technology for passenger cars and can be described as a combination between steer-by-wire and classical power steering. A schematic illustration of the system is shown in Figure 1.1.

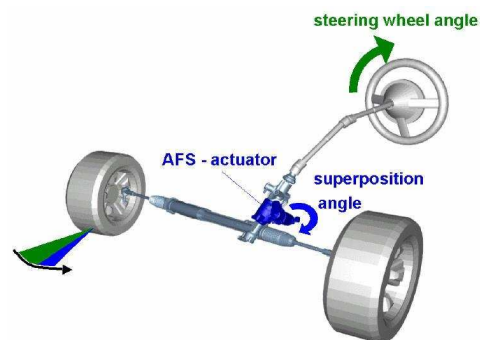


Figure 1.1: A schematic illustration of the AFS system. The steering wheel angle is added to the electric motor angle and the result is driver independent steering interventions at the front wheels.

An electric motor is mechanically connected to the power steering system and an electronically controlled angle can therefore be added (or subtracted) to the

steering wheel angle. The difference from a pure steer-by-wire system is that the mechanical connection between the steering wheel and the road wheels still remains. Hence, a brake down in the AFS electronics will not be fatal for the vehicle's steering abilities.

The principle of the AFS system is shown in Figure 1.2. The driver controls the vehicle via the hand steering wheel and puts out the steering wheel angle δ_S . The AFS system uses its electric motor to actuate the additional angle δ_M . The steering gearset (can be of different type, for example planetary gear) adds the two angles and this results in the final pinion angle δ_G down at the steering rack.

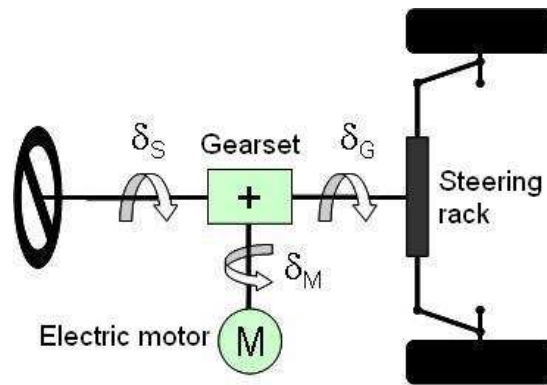


Figure 1.2: The principle of the AFS system is shown in this figure. The gearset adds the steering wheel angle δ_S to the electric motor angle δ_M and the result is the pinion angle δ_G .

Since the AFS system can affect the road wheel angle, independent from the driver's steering actions, an additional degree of freedom for steering dependent driving situations comes up. One example is a function known as *variable steering ratio*. When driving in city traffic, typically keeping a low speed and performing parking maneuvers, the electric motor adds an angle and the driver only has to put in a small steering effort to achieve a large road wheel angle. When driving at higher speeds, typically highways, the electric motor subtracts an angle when the steering effort from the driver becomes large. This helps to keep the vehicle stable during sudden big steering wheel movements. Further, the AFS system can be used to implement convenient functions such as parking assistants and lane keeping.

1.2 Vehicle Dynamic Control

Perhaps the most interesting area of application, for the AFS system, is vehicle dynamic control (vehicle stabilization, VDC). In today's vehicles this is accomplished with different types of electronic stability programs (ESP). Those type of systems uses the brakes to stabilize the vehicle in a critical situation and sometimes that can feel unpleasant for the driver. If the vehicle instead is stabilized with steering interventions, a critical driving situation can be solved

a lot smoother. Also, an electronic steering intervention is accomplished in just a few milliseconds, while building up brake pressure takes over 100 milliseconds, often up to 200 milliseconds.

The control algorithm, for controlling the vehicle in a critical driving situation, is based on the yaw rate $\dot{\psi}$ (therefore it is sometimes simply called yaw rate controller). A desired yaw rate $\dot{\psi}_d$ is calculated in every time sample and the control error e is formed as the difference between the measured and the desired yaw rate. The control signal u is then transformed to a road wheel angle δ_F , which is mapped to a desired AFS motor angle δ_M . The control algorithm signal flow is shown in Figure 1.3. See [1] for a detailed review of vehicle dynamic control with AFS.

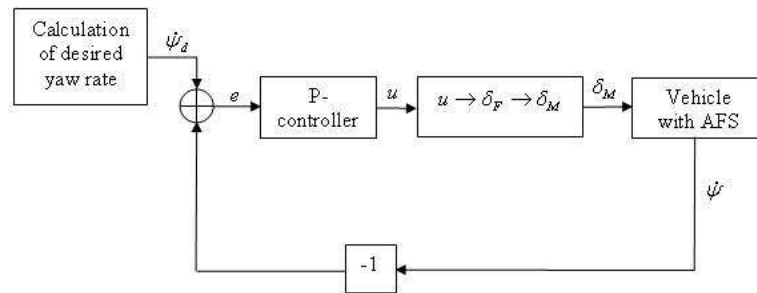


Figure 1.3: In the figure the vehicle dynamic control signal flow is shown. The final controller output is a desired motor angle, which is sent to the AFS system.

The control algorithm is active as soon as the AFS system is active. Though, steering interventions in every time sample is not necessary, so the control signal is taken into account only when the vehicle is said to be in a critical driving situation. A critical situation can be determined in different ways and one way is to use the following equation:

$$a_y \cdot v_x \cdot \ddot{\psi} \geq \eta_{crit} \quad (1.1)$$

where

$$\begin{aligned} a_y &= \text{lateral acceleration,} \\ v_x &= \text{longitudinal velocity,} \\ \ddot{\psi} &= \text{yaw rate derivative and} \\ \eta_{crit} &= \text{critical limit} \end{aligned}$$

The critical limit is a constant value and has to be found through test drives. The problem is that η_{crit} is not of the same magnitude on different road surfaces. If the vehicle is kept on one single type of road surface, determining a critical driving situation with the above equation works fine. But as soon as the road surface changes (the friction coefficient changes) a critical driving situation will not be determined correctly. A more dynamic way to determine a critical situation is to use a concept called *the friction circle*, see Figure 1.4.

The circle boundary is the maximum grip force the vehicle axle i and the current road surface can bring up together. μ_{max} is the road surface friction coefficient

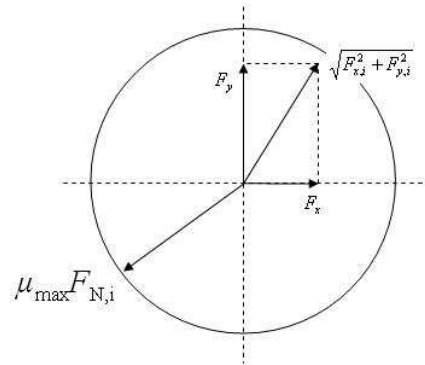


Figure 1.4: The friction circle.

and $F_{N,i}$ the normal force acting on axle i . $F_{x,i}$ and $F_{y,i}$ are the longitudinal and lateral forces acting on axle i . When the combined axle force, $\sqrt{F_{x,i}^2 + F_{y,i}^2}$, is larger than the circle boundary, the vehicle is said to be in a critical driving situation. Equations for how to calculate the vehicle forces can be found in any book on vehicle dynamics, for example [2] or [3]. The problem now consists of how to calculate the friction coefficient and this leads to the main goal with the thesis.

1.3 Thesis Goal

There exists no equations nor formulas for direct calculation of the maximum road-tire friction coefficient. The problem solution is to try to estimate the friction coefficient, in real time, during driving. A reasonable estimation goal is a possible distinction between four different road surfaces; asphalt, gravel, snow and ice. The estimated friction value should then be used as in Section 1.2.

1.4 Friction Estimation Literature Overview

In literature several different friction estimation algorithms are described. Almost all of them are rather complex academic solutions with no real implementation results. These types of algorithms often contain variables and parameters that usually are unknown and very hard to estimate. Some different estimation suggestions can be found in [4], [5], [6], [7] and [8]. Though, also some more useful ideas has been presented. Previous work done by F. Gustafsson, [9] and [10] (based on ideas by T. Dieckmann [11], among others), has been further developed and actually resulted in a selling product which can deliver friction signals corresponding to a few different friction levels. These signals can be used by different systems in the vehicle, for example stability systems, braking systems and torque distribution systems. In this thesis, Gustafsson's estimation suggestions are evaluated, implemented and tested.

In [12] some new ideas, based on the brush model, are presented and evaluated

for friction estimation during the braking case. In this thesis those ideas are reformulated and applied on the driving case.

1.5 Thesis Limitations

While studying the written material concerning friction estimation some time and complexity limitations became obvious. The lateral forces (y -forces) acting on the wheels are very hard to calculate or estimate correctly, therefore the work presented in this thesis only uses longitudinal forces (x -forces) in the estimation procedure. The vehicle direction axles are defined as in Figure 1.5. Some correction factors due to the lateral forces are introduced in the calculations, but physical lateral motion effects such as *slip angle*, *side slip* and *cornering stiffness* are disregarded. Explanations and detailed reviews of these concepts can be found in [2]. Accurate friction estimation during both driving and braking

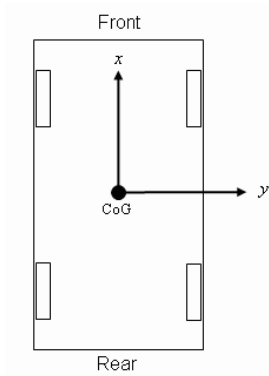


Figure 1.5: The vehicle direction axles.

is not trivial and since the yaw rate controller needs to know the maximum available friction during normal driving, an inclusion of the braking case is left to future work. Discussions on friction estimation during pure braking can be found in several publications, see for example [13], [14] or [15].

Further, all calculations in this thesis are based on a rear wheel driven vehicle, equipped with standard sensors for vehicles with anti-lock braking system (ABS) and sensors for measuring yaw rate and lateral acceleration. Though, the calculations in Section 2.2.2, specific for rear wheel driven vehicles, can easily be adapted to fit front wheel driven vehicles, see [3] and [9]. Finally, as the friction estimation procedures below are formed, they are not suitable for four wheel driven vehicles.

1.6 Thesis Outline

Chapter 2 contains the ideas and equations behind slip-slope based friction estimation. The algorithm is thoroughly reviewed and results from real test drives are presented. Chapter 3 deals with the derivation of the brush model

and how it can be used for direct estimation of the friction coefficient. Results from real test drives are presented also in this chapter. In the last chapter the conclusions, drawn from work presented in this thesis, are stated and discussed. A few topics suitable for future work are also mentioned.

1.7 Basic Notation used in the Thesis

1.7.1 Abbreviations

AFS	Active Front Steering
CAN	Controller Area Network
CoG	Center of Gravity
CUSUM	Cumulative Sum
ABS	Anti-lock Braking System
ESP	Electronic Stability Program
RLS	Recursive Least Squares
VDC	Vehicle Dynamic Control

1.7.2 Variables, Constants and Parameters

s	wheel slip
\hat{s}_{rl}	measured slip for rear left wheel
\hat{s}_{rr}	measured slip for rear right wheel
ω_{fl}	angular velocity for front left wheel
ω_{fr}	angular velocity for front right wheel
ω_{rl}	angular velocity for rear left wheel
ω_{rr}	angular velocity for rear right wheel
v	absolute velocity
v_x	longitudinal absolute velocity
r	wheel radius
μ	friction coefficient
μ_{max}	maximal friction coefficient
F_t	traction force
N	normal force
N_{rl}	normal force acting on rear left wheel
N_{rr}	normal force acting on rear right wheel
k	initial slope of the $u - s$ curve (slip-slope)
δ	slip-slope offset
M_e	engine output torque
ξ_o	transmission overall reduction ratio
η_t	transmission overall efficiency
n_e	engine speed
n_w	average front wheel speed
$\hat{\sigma}^2$	wheel speed variance
p_0	tire pressure
q_z	normal force distribution
a	road-tire contact patch length
σ_x	brush model slip definition

ξ_i	brush element deformation
F_z	brush model normal force
x_c	carcass attachment point
x_{cs}	breakaway point
F_x	brush model longitudinal tire force
C_x	longitudinal tire stiffness
$\sigma_{x,s}$	slip limit
M	vehicle mass
g	gravitational acceleration constant
F_x	longitudinal acceleration force
F_y	lateral acceleration force
F_a	aerodynamic force
b	distance from front axle to the center of gravity
h	height of the center of gravity
L	track width
B	wheel base
$\dot{\psi}$	yaw rate
R	curve radius
ρ	air density
c_d	aerodynamic drag coefficient
A	vehicle frontal area
P_r	air pressure
T_r	air temperature

Chapter 2

Slip-Slope Based Friction Estimation

In this chapter the idea of estimating the road-tire friction by investigating the so called slip-slope will be dealt with.

2.1 Outline and Basics of Slip-Slope Based Friction Estimation

A wheel's angular velocity multiplied by the wheel's radius is known as the wheel's circumferential velocity, wr . If the wheel is non driven, the circumferential velocity is by definition equal to the wheel's absolute velocity, v . The absolute velocity can be defined as the longitudinal velocity of the wheel hub. For a driven wheel will, however, wr not be equal to v . Since a driven wheel is directly connected to the vehicle's power train, a torque can be applied on the wheel. If a positive torque is applied, the wheel will have higher circumferential velocity than absolute velocity. When negative torque is applied on the wheel, the relationship between the two velocities will be the opposite. In reality, wr will be lower than v also for small positive torques. That is, among others, due to the wheel's rolling resistance and inertia. The difference between wr and v , for a driven wheel, is called wheel slip and in [16] defined as

$$s = \frac{\omega r}{v} - 1. \quad (2.1)$$

The same definition is also used in [9] and [10]. It has been shown (see any book in vehicle dynamics, for example [2] or [3]) that the slip is correlated with the friction coefficient μ (also known as the adhesion factor or the normalized traction force), which is defined as the traction force F_t divided by the normal force N

$$\mu = \frac{F_t}{N}. \quad (2.2)$$

An illustration of the different velocities and forces used in slip-slope based friction estimation can be seen in Figure 2.1. The relationship between the slip

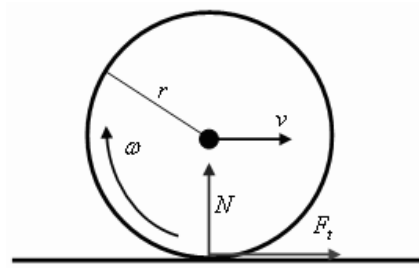


Figure 2.1: Velocities and wheel forces used in slip-slope based friction estimation. ω is the angular velocity, v the longitudinal velocity, r the nominal wheel radius, N the normal force and F_t the traction force.

and the friction coefficient is shown in Figure 2.2. The curves are generated

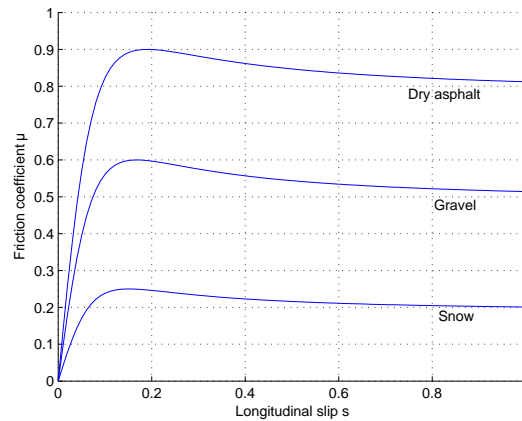


Figure 2.2: The figure shows $\mu - s$ curves for different surfaces, generated with the Magic Formula.

with the well known and in [17] presented empirical formula

$$F(s) = c_1 \sin(c_2 \arctan((1 - c_4)s + (c_4/c_3) \arctan(c_3s))). \quad (2.3)$$

The formula is known as the Magic Formula and is well suited for describing the force–slip relationship. With different parameter sets the formula can describe different types of tires, road conditions and driving circumstances. The coefficients have interpretations as peak factor (c_1), shape factor (c_2), tire stiffness factor (c_3) and curvature factor (c_4). The Magic Formula curve is often used as a reference when the tire force is calculated in some other way, for example as in Section 3.2.

During normal driving only small values $\mu \approx 0.1$ are observed, but the friction that is supposed to be estimated is of course the curve's peak value. That is, the highest amount of friction that can come up between the current road surface and the tire. As seen in the figure the curves are highly nonlinear, but for small

slip values they can be approximated by the linear function

$$\mu = k \cdot s \quad (2.4)$$

where

$$k = \left. \frac{d\mu}{ds} \right|_{\mu=0} \quad (2.5)$$

The curve's slope k in the (approximately) linear area, is known as the tire's longitudinal stiffness and in literature usually said to depend only on tire characteristics (see for example [2]). Though, the hypothesis in slip-slope based friction estimation is that k , further on called the slip-slope, is also depending on the road-tire friction. This hypothesis has, independently from [9] and [11], been confirmed by TNO (an institute for tire testing and research) in the Netherlands and also by various experiments presented in more recent publications, see for example [12]. In order to investigate the slip-slope hypothesis also in this thesis, real measurements were collected during different driving situations and road conditions. In Figure 2.3 the slip and the observed friction coefficient (normalized traction force effort) for driving about 80 km/h on asphalt and snow, respectively, are presented. Both driving cases contains one acceleration and one deceleration phase and data was collected every 10 ms. The snow drive consists of a few more data points and that is due to the slower acceleration abilities that comes with a slippery surface. When straight line is fitted to the data with a least squares approximation, visual inspection reveals a significant difference in the k -value. The slip-slope for the asphalt drive is greater than the one for the snow drive, that is, k grows with the road surface friction coefficient. The friction coefficient for asphalt is approximately 0.9-1.0 and for snow 0.15-0.25, respectively. Friction coefficient values for several different road surfaces can be found in [2].

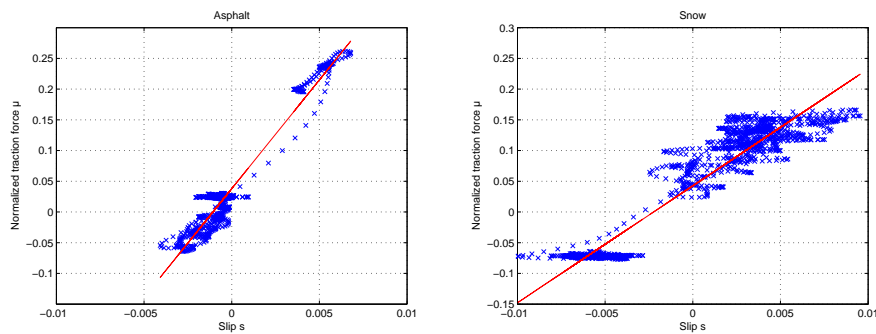


Figure 2.3: Real $\mu - s$ data for dry asphalt and snow, respectively. The solid line, known as the slip-slope, is a least squares straight-line approximation.

2.1.1 Slip-Slope Offset

By inspecting Figure 2.3 closely, a significant offset is discovered,

$$\delta = s|_{\mu=0}. \quad (2.6)$$

In words that means the slip is not zero when the traction force is. This offset is mainly dependent on the rolling resistance of the wheels. Though, in [9] it is said to depend also on slowly time-varying differences in wheel radii. Therefore, the offset can not be given a constant value, instead it has to be estimated in every time sample. When estimating the slip-slope, the estimated offset is then taken into account and compensated for.

2.1.2 Negative Friction Coefficient

In line with the discussion above the deceleration generates a negative slip. As seen in Figure 2.3 also the friction coefficient can take on negative values (in reality negative friction does not exist). That is due to how the traction force is calculated and will be explained later. Though, negative friction coefficient values is a necessity if the friction estimation is supposed to work not only for strictly positive slip values. If the Magic Formula is applied on both negative and positive input data, the $\mu - s$ plot will look like Figure 2.4. By inspecting the figure it is clear that the k -value is the same (for small slip values) whether the data point $\{\mu, s\}$ is located in the first or third quadrant.

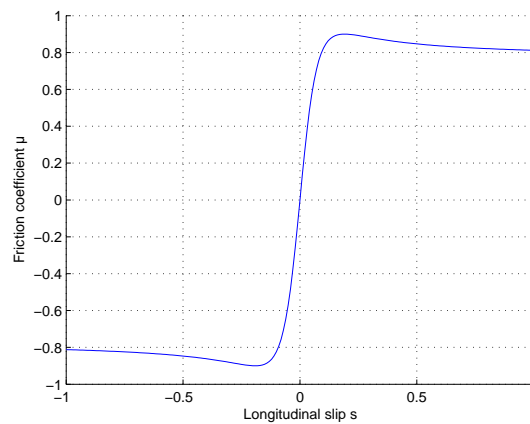


Figure 2.4: Shown in the figure is the $\mu - s$ curve for both positive and negative slip. As seen, the k -value is the same (for small slip values) whether the data point $\{\mu, s\}$ is located in the first or third quadrant.

2.2 Slip-Slope Estimation

In slip-slope based friction estimation there are two main problems to overcome. The first is to come up with a way to online estimate the value of k and the second one is to relate or map that value to an actual friction value. In a real implementation, a distinction between four different road surfaces (for example dry asphalt, gravel, snow and ice) is a reasonable estimation goal.

2.2.1 Linear Regression Model

As previously stated, the goal is to estimate k and δ online. That requires a good linear regression model for which it exists accurate estimation methods. (2.4) is combined with (2.6) and written as

$$\mu = k(s - \delta). \quad (2.7)$$

The negative sign is explained in Section 2.2.2. Since the slip calculations contains much more noise than the friction coefficient calculations, the above model is rewritten as

$$s = \mu \frac{1}{k} + \delta. \quad (2.8)$$

A second good reason for the reformulation is that the parameter δ is varying much slower as compared to $k\delta$. The model is simple, linear in the parameters and therefore suitable for several different online estimation techniques. From Figure 2.3 it is seen that the difference in k -values for different road surfaces is quite small. Hence, the estimation of k (or $\frac{1}{k}$) and δ must be accurate. Still, abrupt changes in k must be detected sufficiently fast. With the δ parameter said to be slowly time varying, the estimation problem consist of parallel parameter tracking with one rapidly and one slowly varying parameter. As mentioned above, several estimation algorithms for this type of problem exists, for example Recursive Least Squares (RLS) and Least Mean Squares (LMS). But the most suitable method is the very well known and widely applied parameter identification Kalman filter. This is because the Kalman filter can be tuned to track model parameters unequally quick (which is not the case for RLS or LMS). If the Kalman filter then is combined with a change detection algorithm, also sudden abrupt changes in k can be detected reasonable fast. See [9] for a more thorough discussion concerning the choice of estimation algorithm.

2.2.2 Kalman Filter Input Calculations

The Kalman filter inputs, the wheel slip and the normalized traction force effort, need to be calculated in every time sample.

Slip Calculation

According to (2.1) the slip calculation needs the absolute velocity of the driven wheels. The absolute velocity is not known and is therefore estimated from the circumferential velocities of the non driven wheels. The slip of the non driven wheels is assumed to be negligible. The slip computation for the left and right side, respectively, is then formed as

$$s_{rl} = \frac{w_{rl}r_{rl}}{w_{fl}r_{fl}} - 1, \quad s_{rr} = \frac{w_{rr}r_{rr}}{w_{fr}r_{fr}} - 1. \quad (2.9)$$

The indices fl , fr , rl and rr stands for front left, front right, rear left and rear right. Since the wheel radii are varying with different load on each wheel, different tire inflation pressure, different worn tires and perhaps other factors,

it can be considered as unknown. Instead the relative difference in wheel radius is defined,

$$\delta_l = 1 - \frac{r_{rl}}{r_{fl}}, \quad \delta_r = 1 - \frac{r_{rr}}{r_{fr}}, \quad (2.10)$$

which, according to [9], can be considered to be the same as the offset in (2.6). Hence, the source of the in Section 2.1.1 visually observed slip-slope offset is derived. Since $\delta_{l,r}$ is unknown the slip measurement quantity \hat{s} is instead defined and given by

$$\hat{s}_{rl} = \frac{w_{rl}}{w_{fl}} - 1, \quad \hat{s}_{rr} = \frac{w_{rr}}{w_{fr}} - 1. \quad (2.11)$$

Equation (2.9) can be written as

$$s_{rl} = \frac{\omega_{rl}}{\omega_{fl}}(1 - \delta_l) - 1 \Leftrightarrow \omega_{rl} = \frac{(s_{rl} + 1)\omega_{fl}}{1 - \delta_l}, \quad (2.12)$$

$$s_{rr} = \frac{\omega_{rr}}{\omega_{fr}}(1 - \delta_r) - 1 \Leftrightarrow \omega_{rr} = \frac{(s_{rr} + 1)\omega_{fr}}{1 - \delta_r} \quad (2.13)$$

and (2.11) as

$$\omega_{rl} = (\hat{s}_{rl} + 1)\omega_{fl}, \quad (2.14)$$

$$\omega_{rr} = (\hat{s}_{rr} + 1)\omega_{fr} \quad (2.15)$$

and by combining (2.12) with (2.14) and (2.13) with (2.15) the relation between the true and the measured slip can be approximated with the expansion

$$\hat{s}_{rl} = \frac{s_{rl} + \delta_l}{1 - \delta_l} = (s_{rl} + \delta_l)(1 + \delta_l + \delta_l^2 + \dots) \approx s_{rl} + \delta_l, \quad (2.16)$$

$$\hat{s}_{rr} = \frac{s_{rr} + \delta_r}{1 - \delta_r} = (s_{rr} + \delta_r)(1 + \delta_r + \delta_r^2 + \dots) \approx s_{rr} + \delta_r. \quad (2.17)$$

As mentioned above, the offset δ can be estimated together with the slip-slope and the Kalman filter slip input becomes

$$s_{rl} = \hat{s}_{rl} - \delta_l, \quad s_{rr} = \hat{s}_{rr} - \delta_r. \quad (2.18)$$

Advanced Absolute Velocity Estimation

Instead of using the angular velocity for the non driven wheel as an estimate for the absolute velocity, an additional approach was investigated. The idea is to simultaneously look at all the four different wheel speeds. The speeds are then filtered, weighted and added together according to the current driving situation. An average value is then formed and used as longitudinal absolute velocity estimation, v_x . This approach turned out to be very robust against wheel spin, hard braking and skidding and where therefore used as absolute velocity throughout this entire project. Since the wheel speeds, extracted from the CAN-bus of the prototype car, are delivered as circumferential velocity measurements, the slip measurement equations instead becomes

$$\hat{s}_{rl} = \frac{w_{rl}r_{rl}}{v_x} - 1, \quad \hat{s}_{rr} = \frac{w_{rr}r_{rr}}{v_x} - 1. \quad (2.19)$$

The wheel radii are still not known and when this report was written it was not entirely clear how the car manufacturer solved that problem. Probably the wheel radii are given nominal values that are used throughout the entire life cycle of the car.

Empirical investigations revealed that the slip-slope offset δ still showed up in a similar way as before. That is explained with the fact that v_x is formed directly from the different wheel speeds (which are delivered as circumferential velocities assumptively based on nominal wheel radii). So (2.16) and (2.17) are assumed to still hold.

Traction Force Calculation

With the inertia of the wheels and driveline neglected, the longitudinal road-tire traction force effort F_t , can be calculated as

$$F_t = \frac{M_e \xi_o \eta_t}{2r} \quad (2.20)$$

where

$$\begin{aligned} M_e &= \text{engine output torque,} \\ \xi_o &= \text{transmission overall reduction ratio,} \\ \eta_t &= \text{transmission overall efficiency and} \\ r &= \text{tire radius.} \end{aligned}$$

The factor 2 in the denominator comes from the assumption that the final drive (differential gear) divides the torque, available after the gear box, equal between the two driven wheels. The transmission overall reduction ratio (combined gear ratio and final drive ratio) together with the overall efficiency is calculated by comparing the engine speed with the speed of the non driven wheels,

$$\xi \cdot \eta_t = \frac{n_e}{n_w}. \quad (2.21)$$

n_e is the engine speed and n_w the averaged wheel speed converted to revolutions per minute. The reason why negative traction force can be observed is dependent on the engine torque measurements. When no torque is transferred from the engine to the wheels (no throttle is given) the internal friction in the engine will result in a negative torque. The engine friction gives a torque contribution of approximately -10 Nm per liter displacement volume. If the inertia of the wheels and the driveline is known, the traction force calculation can be made more accurate. Formulas for that can be found in [3].

Normal Force Calculation

Since the slip is related to the *normalized* traction force (the friction coefficient) the normal forces acting on the driven wheels needs to be calculated. The

normal forces are given by

$$N_{rl} = \frac{Mg \cdot b + h(F_x + F_a) - 2F_y \cdot \frac{h}{L} \cdot b}{2B} \quad (2.22)$$

$$N_{rr} = \frac{Mg \cdot b + h(F_x + F_a) + 2F_y \cdot \frac{h}{L} \cdot b}{2B} \quad (2.23)$$

where

- Mg = weight of the vehicle,
- F_x = longitudinal acceleration force,
- F_y = lateral acceleration force,
- F_a = aerodynamic force,
- b = distance from the front axle to the CoG,
- h = height of the CoG,
- L = track width and
- B = wheel base.

In Appendix A.2 a detailed derivation is given.

The normalized traction force effort is then calculated as in (2.2).

2.2.3 The Discrete Optimal Kalman Filter

With the required filter input values at hand, the unknown model parameters k and δ can be estimated. The friction model (2.8) is reformulated into a state space model

$$\theta_{k+1} = \theta_k + v_k \quad (2.24)$$

$$s_k = \varphi_k^T \theta_k + e_k \quad (2.25)$$

where

$$\theta_k = \begin{pmatrix} \frac{1}{k_k} & \delta_k \end{pmatrix}^T$$

$$\varphi_k = \begin{pmatrix} \mu_k & 1 \end{pmatrix}^T.$$

s_k and μ_k are calculated according to (2.19) and (2.2), respectively. v_k and e_k are considered as independent white noise processes with covariances

$$Q_k = E \{v_k v_k^T\}$$

$$R_k = E \{e_k e_k^T\}.$$

The optimal (in the minimum variance sense) parameter estimates are now given by the Kalman filter

$$\hat{\theta}_{k+1} = \hat{\theta}_k + K_k \left(s_k - \varphi_k^T \hat{\theta}_k \right) \quad (2.26)$$

$$K_k = P_k \varphi_k \left(R + \varphi_k^T P_k \varphi_k \right)^{-1} \quad (2.27)$$

$$P_{k+1} = P_k + Q - P_k \varphi_k \left(R + \varphi_k^T P_k \varphi_k \right)^{-1} \varphi_k^T P_k. \quad (2.28)$$

As seen in the equations, the time indices are dropped for the Kalman filter tuning parameters Q and R . This is done since there is no *a priori* information about when to expect large variance changes in the estimates. If R is normalized ($R = I$), the diagonal elements in Q determine the filter time constant and tracking speed for k and δ . Detailed reviews of the Kalman filter and other online parameter identification algorithms can be found in [18] and [19].

In the real implementation, one filter for each driven wheel is used. The final k -value estimate is then formed as the average value of the two filter outputs. This approach makes the system fairly robust against sudden and unexpected disturbances.

2.2.4 Filtering of Measurement Signals

All the sensor signals are subjected to quite heavy measurement noise. This is especially noticed in the slip calculations where the wheel speed measurement noise is amplified. Therefore all the measurement signals are low pass filtered before they enter the estimation. The filter has to be designed in such a way that disturbances from unevennesses in the road and similar factors do not affect the estimation. At the same time, important information can not be afforded to be lost. Hence, the filter cut off frequency has to be chosen wisely. Since the friction estimation is based on the relationship between the slip calculation and the friction coefficient calculation, it is important not to introduce phase shifts between the filtered measurement signals. That is, the signals should be filtered with the same filter. The filter used in the real implementation is a basic second order filter with the continuous time structure

$$G(s) = \frac{\beta^2}{s^2 + \sigma\beta s + \beta^2}. \quad (2.29)$$

In Figure 2.5 the bode plot for the filter is shown. As seen, the cut off frequency is around 20 Hz and the frequency components over that frequency are effectively damped out. The cut-off level was chosen after basic trial-and-error experiments. A better, but more time consuming approach, would be to do a frequency analysis of the interesting signals and then design a filter based on that knowledge.

The output from a second order filter will always oscillate right after t_0 , but since the oscillations are damped out within a second they will not cause any problems in the parameter estimation.

2.3 Algorithm Details and Friction Estimation Results

2.3.1 The CUSUM Detector

As discussed in Section 2.2.1, the Kalman filter needs to be relatively slow (small values on the entries of Q) to be able to track small variations in the estimates. This requirement result in that major road-tire friction changes may not be

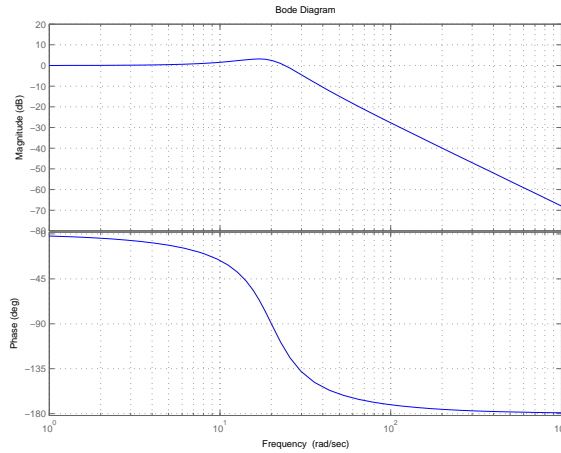


Figure 2.5: Bode plot for the second order low pass filter used in the estimation procedure.

noticed sufficiently fast. Though, the problem can be solved by making the Kalman filter adaptive. If a change detection algorithm is running in parallel with the filter, the algorithm can signal when something has changed. The entries of Q are then momentarily increased and the adaptive Kalman filter will converge much faster as compared to the non adaptive. It exists several different change detection algorithms, see [18] for a thorough review. In [9] some of the algorithms available are tested and evaluated. The one which gave the most promising result, when concerning the combination of the aspects good result, implementation trivialness and type of application environment, was the CUSUM algorithm. The CUSUM algorithm is given below:

$$\begin{aligned}
 g_0 &= 0 \\
 g_t &= g_{t-1} + \epsilon_t - \nu \\
 g_t &= \max(g_t, 0) \\
 g_t &= 0, \text{ and increase } Q \text{ if } g_t > h > 0
 \end{aligned}$$

The algorithm has three inputs; the Kalman filter prediction errors $\epsilon_k = \hat{s}_k - \varphi_k \hat{\theta}_k$, the detection threshold h and the algorithm drift preventer ν . If the algorithm is stated as above, sudden *decreases* in the friction will be detected. A parallel running algorithm with different sign before ϵ_k also makes friction *increases* detectable. A simulation was performed to investigate the influence of the CUSUM algorithm. μ -data based on real measurements were used to generate corresponding slip data from the model described in (2.8). A k -value change from 40 to 30 (friction decrease) was included in the slip data generation. The slip offset δ was given a constant value of 0.005 and additive white noise with variance 10^{-7} was used to simulate the slip noise (the same type of simulation procedure as in [10]). When a change was detected the Q -element corresponding to k was momentarily multiplied by a factor of 50 (can be any value). In theory and in simulations with “good” data, the multiplication factor has no upper limit and the Kalman filter can be made infinite fast. In a real implementation the factor has to be tuned according to test drive results. A too large “ Q -gain”

can result in sudden losses of tracking accuracy. In Figure 2.6 the result of the simulation is shown. Clearly, the CUSUM algorithm improves the convergence rate of the Kalman filter.

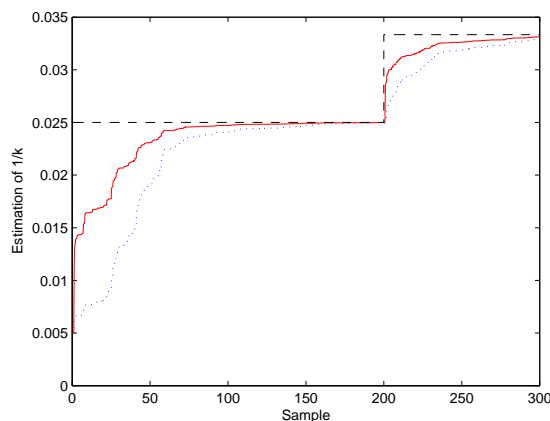


Figure 2.6: Simulation based $1/k$ -estimations with (solid line) and without (dotted line) a change detector. The dashed line is the true $1/k$ -value.

The actual behavior of the algorithm is shown in Figure 2.7. As seen, the algorithm performs as intended and the Q -element corresponding to the k -value is increased when the predictions errors have been sufficiently positive for a while. The algorithm parameters h and ν were hand tuned to fit the simulation data. In a real implementation the algorithm parameter tuning becomes a quite tricky problem. This is due to the fact that sudden friction changes do not always generate prediction errors with the same magnitude. A solution to this problem could be, in some way, to make the detection threshold parameter adaptive and dependent on the probability for a certain prediction error level.

2.3.2 Gravel Detection

Previously empirical studies, [9], have shown that the slip-slope for gravel roads can take on almost any value (also noticed in this thesis). Gravel and rough roads are therefore more or less impossible to classify only by investigating the slip-slope. The solution idea to this problem is to take advantage of the rough surface of a gravel roads and other rough roads. All the small unevennesses in the road will show up as an additive error term in the wheel speed measurements. According to the central limit theorem this error will be Gaussian. By comparing the non filtered wheel speeds of the non driven wheels, the wheel speed variance can be estimated. The hypothesis is that this variance, for gravel, will be distinct larger (due to the error term) than the same variances for other types of road surfaces. The variance is estimated with the following equation:

$$\hat{\sigma}^2 = E \{ \omega_{fl}(t) - \omega_{fr}(t) - \omega_{fl}(t-5) + \omega_{fr}(t-5) \}^2. \quad (2.30)$$

The reason why time $t-5$ is used is due to the prototype car's relatively small sample time (10 ms). The differences in the wheel speeds, if $t-1$ is used,

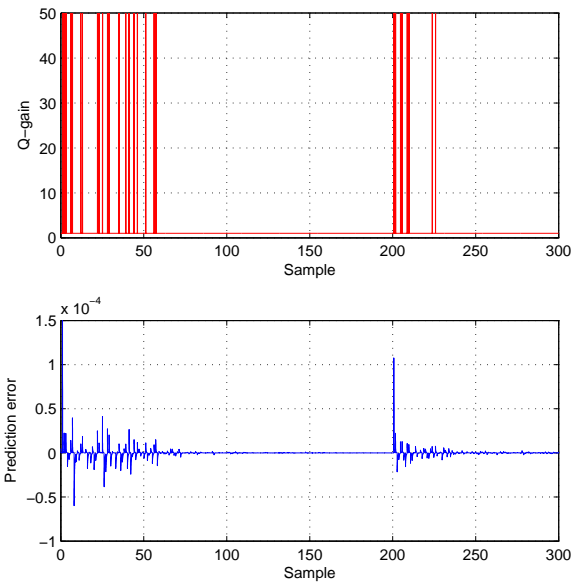


Figure 2.7: When the prediction errors have been sufficiently positive for a while, the CUSUM algorithm momentarily increases the Q element corresponding to the k -value.

will not be large enough to ensure a reliable and usable variance estimation. In Figure 2.8 the variance estimation during a transition from gravel to dry asphalt (approximately at $t = 220$) is shown. The proposed gravel/rough road detection ideas seems to work perfectly as intended and there is a clear difference between the estimated gravel and asphalt variances.

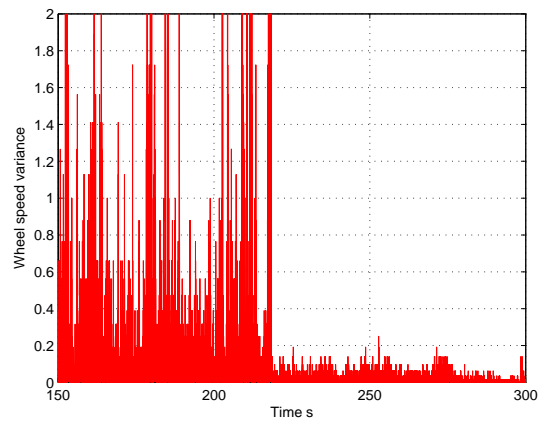


Figure 2.8: Wheel speed variance estimation during a road surface change from gravel to asphalt.

2.3.3 Estimation Results

A lot of real measurement data was collected at different proving grounds and on different road surfaces; the test track at ZF Lenksysteme in Schwäbisch Gmünd (asphalt), Bosch's test track in Boxberg (dry asphalt, wet asphalt, gravel and special slippery surfaces), at Bosch's Test Center in Arjeplog (asphalt, snow and ice) and during driving on public roads and highways around Schwäbisch Gmünd. While driving on public roads the active steering was disconnected and only data gathering was performed. The measurements are collected via a special hardware that is connected directly to the car's CAN-bus. The data is then converted to a format suitable for system development. The needed signals are fed into a structure, which is implementing the estimation ideas above. There is not unlimited amount of data storage memory available in the measurement hardware, so only shorter test drives (a couple of hundred seconds) can be used to investigate the system off-line. But since all data is "recorded" a test drive can be fully reconstructed off-line. The test drives on snow and ice (Arjeplog Test Center) were mainly limited by the size of the test track and mostly could not be made longer than 20-30 seconds. Further, the time and seasonal circumstances of this thesis resulted in that not all types of winter test drives could be performed.

By studying the off-line behavior, effects of small algorithm adjustments can be investigated directly. The Kalman filter performance investigation and tuning of its parameters are preferably also done off-line. A typical system behavior, when the algorithm has been tuned, is shown in Figure 2.9.

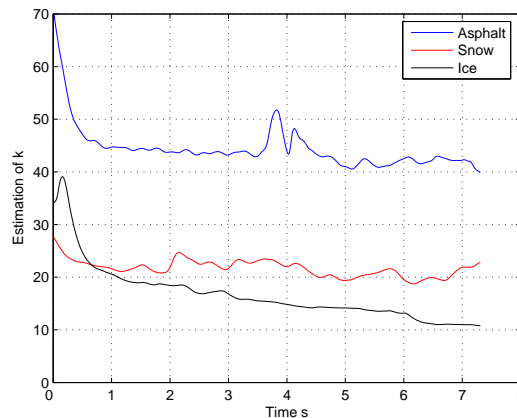


Figure 2.9: The figure shows estimations of the slip-slope, based on real measurement data, for three different road surfaces.

As clearly seen, the Kalman filter work as intended and there is a distinct difference between the estimated slip-slopes for the different surfaces. In line with the hypothesis in Section 2.1 a high friction road surface corresponds to a large k and a low friction surface to a small k . The estimation of k is filtered with an exponential moving average filter having a time constant of half a second. A moving average filter effectively smoothes out unwanted estimation fluctuations.

The filter is described by the equation

$$y(t) = y(t-1) + K(u(t) - y(t-1)) \quad (2.31)$$

where

$$K = \frac{2}{N+1} \quad (2.32)$$

and where N is the number of previous values used in the filtering.

Probably the most important aspect of a friction estimator is that it should be able to detect abrupt friction changes reasonable fast. In Figure 2.10 a sudden surface change from dry asphalt to ice is shown.

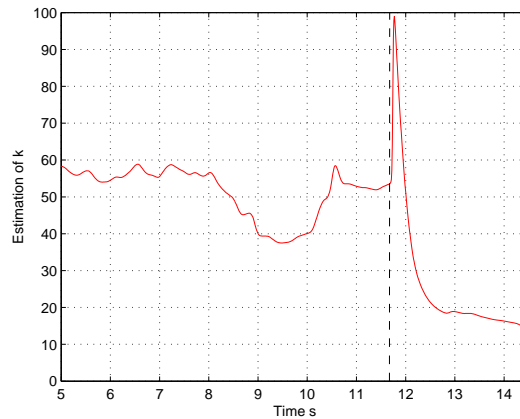


Figure 2.10: Estimation of the slip-slope, based on real measurement data, for a sudden road surface change from dry asphalt to ice. The surface change is marked by the dashed line.

As seen, the system response is quick and the estimation converges to a new lower k -value in approximately one second. Since the Kalman filter must be tuned to be quick, sudden large changes in input data can result in transient effects (also seen in Figure 2.10).

Figure 2.11 shows the behavior of the CUSUM algorithm for the same surface change as above. The algorithm successfully detects the sudden larger prediction errors and momentarily increases the Q -element corresponding to the k -value.

If an exponential moving average filter is applied on the wheel speed variance estimation, a significant threshold for detecting gravel is revealed. In Figure 2.12 the filtered version of the above mentioned gravel to asphalt change is displayed. Also the estimated wheel speed variances for test drives on a public road (asphalt) and on a snow/ice track are shown.

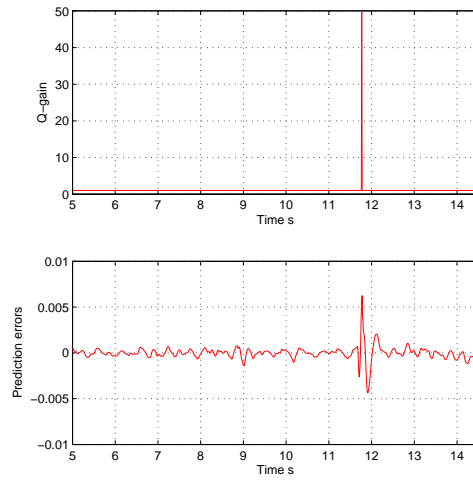


Figure 2.11: The CUSUM algorithm successfully detects the sudden “big” prediction errors and momentarily increases the Q -element corresponding to the k -value.

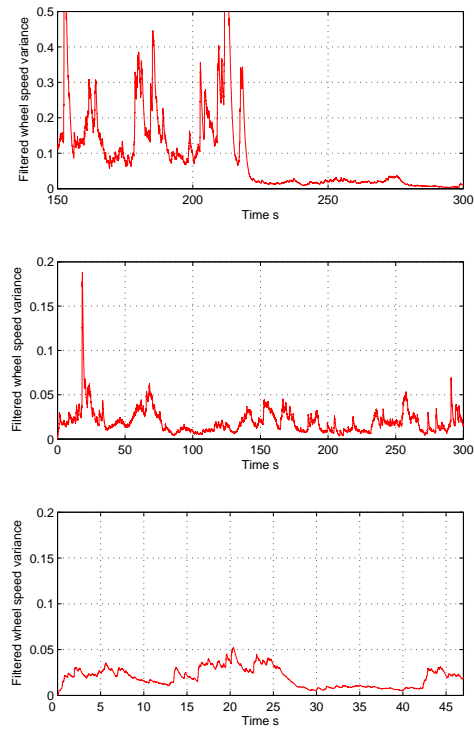


Figure 2.12: Upper plot: the filtered wheel speed variance estimation during a surface transition from gravel to asphalt. Middle plot: the variance during a test drive on an asphalted public road. Lower plot: the variance during a test drive on a snow/ice track. Clearly, a distinction between gravel and other surfaces can be made by investigating the wheel speed variance.

With the estimation results at hand it is seen that the slip-slope based friction estimation algorithm can be used to distinguish between at least three different road surfaces/friction levels. The differences in the estimated k -values are definitely large enough to separate a high friction surface (asphalt/concrete, $\mu_{max} \approx 0.9 - 1.0$) from a surface with low friction (snow/ice, $\mu_{max} \approx 0.1 - 0.2$). The gravel/rough road detector gives the third and intermediate friction level, $\mu_{max} \approx 0.5 - 0.6$. As mentioned, friction levels for different road surfaces can be found in [2].

2.3.4 Calculating the Friction Coefficient while ABS Braking

As stated in [9], a rough way to quickly estimate the friction coefficient is to measure the mean deceleration while performing an ABS braking. This approach is of course not usable as a friction estimator in a real implementation, but it can be used as a reference when designing a function or lookup table for mapping slip-slope to friction. Modern vehicles, equipped with ABS, have a hardware flag that is raised when the ABS is active. So, if an ABS braking starts at time t_1 and ends at time t_2 an estimate of the friction coefficient is given by

$$\mu_{max} = -\frac{\dot{v}_x}{g} \approx -\frac{v_x(t_2) - v_x(t_1)}{g} \quad (2.33)$$

2.3.5 Algorithm Details

Since the friction model used in the estimation procedure is valid only in a certain region (low slip and normalized traction force values, recall Section 2.1), the data fed into the Kalman filter must be carefully chosen. The filter needs a continuously flow of data, so data from outside the valid region can not just be thrown away. This problem is solved by an enable signal calculation. The enable signal is calculated prior to the filter and the binary on/off value is then simply fed into it. When the enable calculation discovers non usable data the filter is notified and put in “idle” mode. The filter will now repeatedly feed it self with the last good input data until the enable signal becomes high again. During non valid data periods the filter states are not updated and simply keep the values corresponding to the last good input data.

Enable Signal Calculation

The enable signal calculation is built as a simple logic structure with one binary output. The signals, that the friction model is dependent on, are checked in every sample and if one or more of them are outside the predefined validity area, the enable signal becomes low.

Since the observed friction coefficient is directly proportional to the engine torque, the torque needs to be monitored. Abrupt and large changes in the torque will have negative influence on the estimation. Such changes are typical generated when the clutch is pressed and no torque is transferred from the engine to the wheels. As proposed in [20], this can be handled by monitoring

the gear ratio. Each gear corresponds to a certain gear ratio, calculated from (2.21). The computation of the gear ratio will start to drift when the clutch is pressed. An open clutch can then be detected by having predefined working intervals for every gear. A gear ratio not located within any of the allowed intervals will result in a low enable signal. A test drive containing gear changes from 1st to 6th gear is shown in Figure 2.13. As can be seen in the figure, a gear change from, for example, 5th to 2nd gear will result in a gear ratio calculation crossing two non interesting intervals. To keep the enable signal constantly low during such gear changes, a hysteresis is introduced. The clutch is said to be open until the gear ratio calculation has been stable, within an allowed interval, during some specific time. Also included in the figure below is the enable signal during the gear changes. Large engine torque changes, with the clutch closed, are discovered by studying the torque derivative.

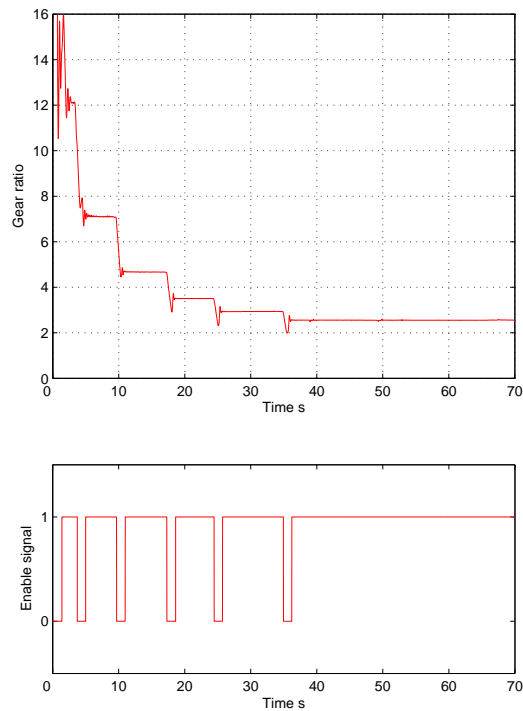


Figure 2.13: Upper plot: Gear ratio calculation output during gear changes from 1st to 6th gear. The non exactness for the first gear is due to the fairly high amount of clutch slipping. Lower plot: The enable signal during the gear changes.

As the traction force effort is calculated (2.20), the k -estimation will not work while the brakes are in use. Since a braking situation will result in a $\{\mu, s\}$ data point not located on the linear part of the $\mu - s$ -curve, the accuracy of the estimation will be lost. The slip magnitude, with negative sign, will still be accurate, but the traction force effort calculation will not be correct. The problem is handled by continuously checking the applied brake pressure. When the pressure goes from zero to positive, the enable signal becomes low.

Chapter 3

Brush Model Based Friction Estimation

The brush model aims at describing the forces generated in the tire and between the tire and the road. The model is based on physical observations and derivations and therefore contain parameters with clear interpretations. Hence, the brush model is more easy to adapt to different circumstances than today's popular empirical models (for example the Magic Formula). The model presented in this chapter will be restricted to the longitudinal case and the modeling will consist of the basic equations the brush model is based on. For a more detailed review, which also deals with lateral forces see [12].

3.1 Tire Modeling

The simple force-slip model, used in slip-slope based friction estimation, is based only on observed phenomena and the derivation does not try to explain how the forces come up. Further, the linear model is valid only for small slip values. The brush model, on the other hand, tries to describe the tire forces for all slip values and explain how, why and where the forces are generated. This requires knowledge about how tires are built up and how they react to external forces.

As stated in [13], a tire mainly has two purposes; to transmit forces between the road and the vehicle body and to work as an active component in the suspension system. For example, tires are designed to reduce the high frequency vibrations from the small unevennesses in the road. Since a tire is a very complex and nonlinear structure, a precise modeling requires highly advanced modeling techniques. Such models are not useful in real implementations and barely even in pure simulations. Therefore, a lot of work has been done to derive more simple models with few parameters, see for example [17]. A summary of the work done in the 60's and 70's can be found in [21]. In the last two decades, purely empirical models have been popular among researchers and vehicle system developers. These models can be very well fitted to data for a certain tire during some well defined driving circumstance. The different forces can then be calculated fairly accurate. Though, the major drawback is that

those models are more or less useful only in offline simulations. A lot of today's vehicle safety systems would, of course, perform better if the tire forces could be estimated and predicted, online, in an accurate way. This has lately made physical tire models more attractive since they contain real physical parameters with clear interpretations.

When a tire is exposed to a vertical load it will deform. This deformation is a must if the tire should be able to maintain its good characteristics, but it makes the modeling considerable harder. A common simplification is that the tire air pressure will remain constant during deformation. This means that the deformation is assumed to take place only in the tire rubber. To enhance the modeling accuracy, the vertical force (the normal force) is assumed to be applied not just at a single point, but instead over some geometric area. This area is known as the road-tire contact patch, [13]. When the wheel is not moving the pressure $q_z(x)$ between the tire and the road normally can not exceed the tire air pressure, p_0 . In the center of the contact patch there is an area where the pressure is equal to p_0 . At the ends of the contact patch the pressure smoothly decreases from p_0 to 0. An illustration of the pressure distribution in a longitudinal cut of a tire can be seen in Figure 3.1. The pressure distribution in the lateral

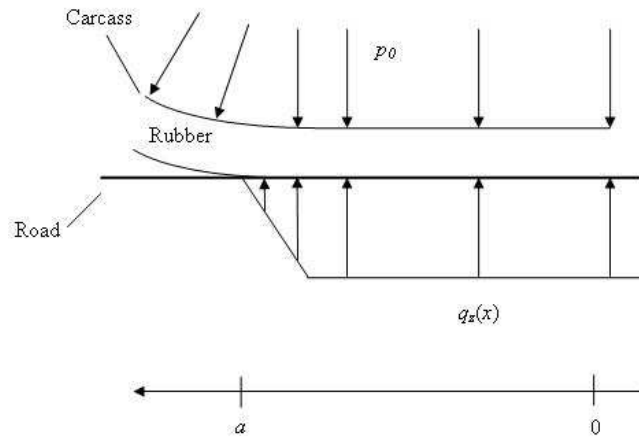


Figure 3.1: The figure shows the longitudinal pressure distribution. The tire pressure p_0 is constant while the pressure between the tire and road $q_z(x)$ decreases toward the ends.

direction depends on how well inflated the tire is. The inflation pressure affects the shape of the carcass, which decides the shape of the contact patch. Basically, the contact patch, in the lateral direction, can take on two different forms. A well inflated tire result in a round contact patch and a poorly inflated tire gives a more rectangular form. The two types of lateral pressure distribution can be seen in Figure 3.2. A common and realistic assumption is to treat the lateral deformation as an intermediate mix between the the two geometric shapes. As mentioned, a more thorough discussion can be found in [12].

For a moving tire the pressure distribution will no longer be symmetric. A rolling tire continuously deforms and a braking torque will be developed. The center of the pressure distribution will move forward, so the pressure will increase in

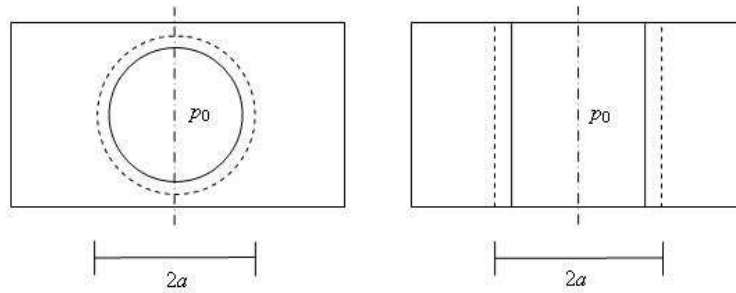


Figure 3.2: In the figures the lateral pressure distribution is shown. The left figure corresponds to a well inflated tire and the right figure to a poorly inflated. The road-tire pressure is p_0 inside the solid line and decreases to 0 at the dashed line.

the first half of the contact patch. This is the source of the rolling resistance. When an external force is applied at the tire (driving, braking or cornering) the center of the pressure will move, within the contact patch, in a nonlinear way. Since this phenomena is depending on the velocity, the damping and the mass of the deformed rubber, it is hard to model. Though, usually the vertical force center is assumed to move in the opposite direction of which the external force is working. For example, a driving force (traction force) will result in a vertical force center located further back in the contact patch. See [2] for more details.

In line with the discussion above, the pressure distribution is commonly given as a parabolic function of the longitudinal coordinate x . At stand still, the peak of the function is located at the center of the contact patch.

3.2 The Brush Model

The source of the tire forces is in the brush model assumed to be the deformation of the rubber. Further, the deformations in the tire contact patch correspond to the slip. The slip definition here is a bit different from the one used in slip-slope based friction estimation. Since the calculations in this thesis are restricted to the longitudinal case, the slip is assumed to depend only on the driving or braking torque working on the wheel. The slip is given by

$$\sigma_x = \frac{v_x - \omega r}{\omega r}. \quad (3.1)$$

The basic idea, in the brush model, is to approximate the rubber volume with small, independently, deformable brush elements. These elements are said to be attached to the carcass, which is assumed to be solid and stiff. Though, the carcass can still flex towards the wheel hub, see Figure 3.3. A brush element i comes in contact with the road at time $t = 0$ and at the contact patch position $x = a$. The deformation of a specific element is given by

$$\xi_i = x_{ci} - x_{ri}. \quad (3.2)$$

x_{ci} and x_{ri} are the contact patch positions where the element is attached to the carcass (index ci) and the road (index ri), respectively. The positions are given

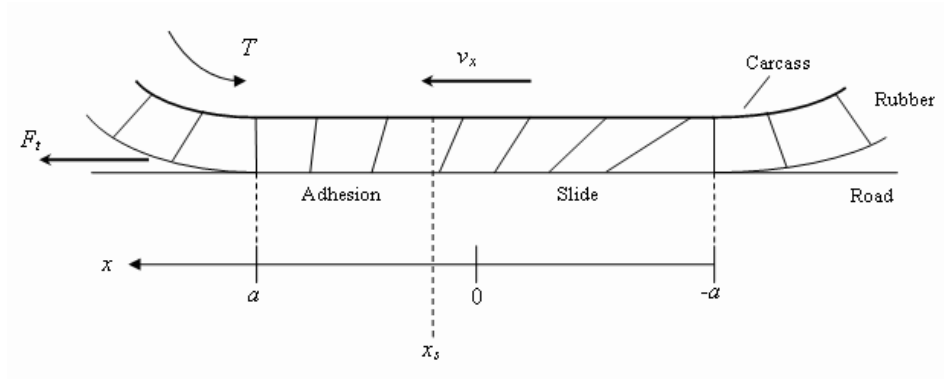


Figure 3.3: In the brush model the tire rubber deformation is modeled as in the figure. T is the available torque at the end of the power train.

by

$$x_{ci} = a - \int_0^t \omega r dt \quad (3.3)$$

$$x_{ri} = a - \int_0^t v_x dt \quad (3.4)$$

where the radius r is defined as the radius from the wheel hub to the carcass. The element deformation can then be written as

$$\xi_i = \int_0^t v_x - \omega r dt \quad (3.5)$$

and if constant velocities are assumed while an element travels through the contact patch, the above equations gives

$$\xi_i = \sigma_x (a - x_{ci}) = \frac{v_x - \omega r}{v_x} (a - x_{ri}). \quad (3.6)$$

A fairly important approximation in the brush model is that rubber is said to deform linearly, [13]. With that approximation the force needed to achieve the amount of deformation given in (3.2) then is

$$F_{xi} = k \xi_i \quad (3.7)$$

The maximum force that can act on a brush element is solely dependent on the road-tire friction and given by

$$F_{xi,max} = \mu F_{zi} \quad (3.8)$$

where F_{zi} is the vertical force acting on the brush element. The maximal element deformation can then be calculated as

$$\xi_{i,max} = \frac{\mu F_{zi}}{k}. \quad (3.9)$$

It is trivial to realize that the brush element starts to slide on the road surface when the deformation reaches the above value. Hence, the contact patch can

take on three different “looks”: There can be adhesion over the entire patch, the rubber within the patch can be fully sliding on the road, or there can be a mix between sliding and adhesion. Again, see Figure 3.3.

If there is a mix between adhesion and sliding, the point (the breakaway point) where the brush element goes from adhering the road surface to slide on it, can be calculated as (by setting (3.6) equal to (3.9))

$$x_{cis} = a - \frac{\mu F_{zi} \omega r}{k(v_x - \omega r)} \quad (3.10)$$

When the breakaway point and the force acting on a specific element are known, the total driving (or braking) force can be calculated. Two physical parameter changes are made: $k = c_p dx_c$ and $F_{zi} = q_z(x_c) dx_c$, where c_p denotes the element stiffness per length unit and q_z , as before, the road-tire vertical pressure distribution per length unit. Adding the force from the area of adhesion to the force from the sliding region and integrating over the entire contact patch (element index i is dropped) the total longitudinal force becomes

$$F_x = \int_{x_{cs}}^a c_p \frac{v_x - \omega r}{\omega r} (a - x_c) dx_c + \int_{-a}^{x_{cs}} q_z(x_c) \mu dx_c. \quad (3.11)$$

As mentioned, the vertical pressure distribution is usually described as a parabolic function and can be written as

$$q_z(x_c) = \frac{3F_z}{4a} \left(1 - \left(\frac{x_c}{a} \right)^2 \right). \quad (3.12)$$

By solving the integrals in (3.11), the final expression for the longitudinal force becomes

$$F_x = 2c_p a^2 \sigma_x - \frac{4}{3} \frac{(c_p a^2 \sigma_x)^2}{\mu F_z} + \frac{8}{27} \frac{(c_p a^2 \sigma_x)^3}{(\mu F_z)^2}. \quad (3.13)$$

In the above expression, $2c_p a^2$ equals the k -value in slip-slope based friction estimation. Though, in the brush model it is usually denoted C_x . Hence, the longitudinal force can be written as

$$F_x = C_x \sigma_x - \frac{1}{3} \frac{(C_x \sigma_x)^2}{\mu F_z} + \frac{1}{27} \frac{(C_x \sigma_x)^3}{(\mu F_z)^2}. \quad (3.14)$$

When the slip becomes sufficiently high, the entire contact patch will slide on the road surface. This slip value is given by

$$\sigma_{x,s} = \frac{3\mu F_z}{C_x}. \quad (3.15)$$

When the slip exceeds this value, the force F_x will be put to μF_z . In Figure 3.4 a $\mu - s$ plot based on the brush model is shown. Also included in the plot are the same curves generated with the Magic Formula. As clearly seen, the brush model can be adjusted in such a way that it perfectly fits the Magic Formula up to the brush model slip limit. Since *normal* driving corresponds to $\{\mu, s\}$ data points located below the slip limit, an agreement above the limit is not necessary.

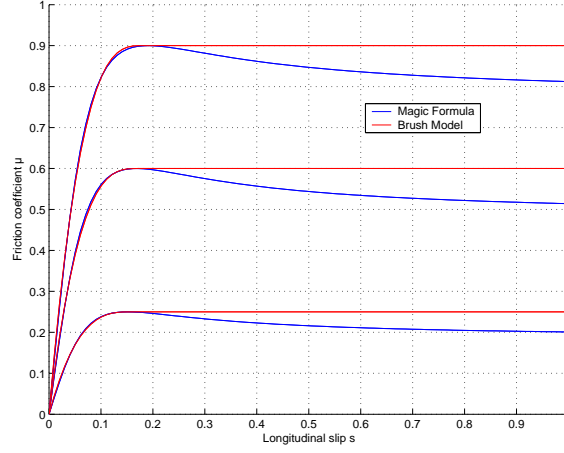


Figure 3.4: The figure shows a $\mu - s$ plot generated with the brush model. The magic formula is used as a reference curve.

3.3 Friction Estimation with the Brush Model

Since the maximal available road-tire friction is explicitly included in the brush model, it is, at least in theory, possible to estimate it directly. A slightly reformulation of (3.14) makes a parametrization possible. By dividing the entire expression with the normal force F_z the brush model becomes

$$\frac{F_x}{F_z} = \mu = \frac{C_x}{F_z} \sigma_x - \frac{C_x^2}{3\mu_{max} F_z^2} \sigma_x^2 + \frac{C_x^3}{27\mu_{max}^2 F_z^3} \sigma_x^3, \quad (3.16)$$

where μ is the normalized traction effort (observed friction coefficient) and μ_{max} the maximal available friction. The above equation can be written on linear regression form as $y_k = \varphi_k^T \theta + e_k$. And by choosing the regression vector and the parameter vector as

$$\varphi_k = \begin{pmatrix} \sigma_{x,k} \\ -\frac{\sigma_{x,k}^2}{3} \\ \frac{\sigma_{x,k}^3}{27} \end{pmatrix}, \quad \theta = \begin{pmatrix} \theta_0 \\ \theta_1 \\ \theta_2 \end{pmatrix} = \begin{pmatrix} \frac{C_x}{F_z} \\ \frac{C_x^2}{F_z^2 \mu_{max}} \\ \frac{C_x^3}{F_z^3 \mu_{max}^2} \end{pmatrix}, \quad (3.17)$$

the maximal available friction can, for example, be derived as

$$\mu_{max,1} = \frac{\theta_0^2}{\theta_1} \quad (3.18)$$

or

$$\mu_{max,2} = \sqrt{\frac{\theta_0^3}{\theta_2}}. \quad (3.19)$$

Since the second μ_{max} calculation contains a square root it should be used with carefulness. Sudden fluctuations in the estimates can result in a square root of a negative value.

The estimation procedure, while using the brush model, is very much similar to the slip-slope case. The inputs, again are, the slip (in this case σ_x according to (3.1)) and the normalized traction force effort ((2.20) combined with (2.22) or (2.23)). Estimation results from test drives on snow covered ice and on dry asphalt are shown in Figure 3.5. The data was gathered during soft accelerations. As seen, the estimation on the slippery surface is more robust and that is probably due to the higher slip values generated on snow/ice. But, direct friction estimation with the brush model seems to be fairly accurate and there is a distinct difference between the estimated friction coefficients for the two road surfaces. It should be said though, that precise friction estimation with the brush model requires very good slip and traction force values, which is mostly not the case during normal driving.

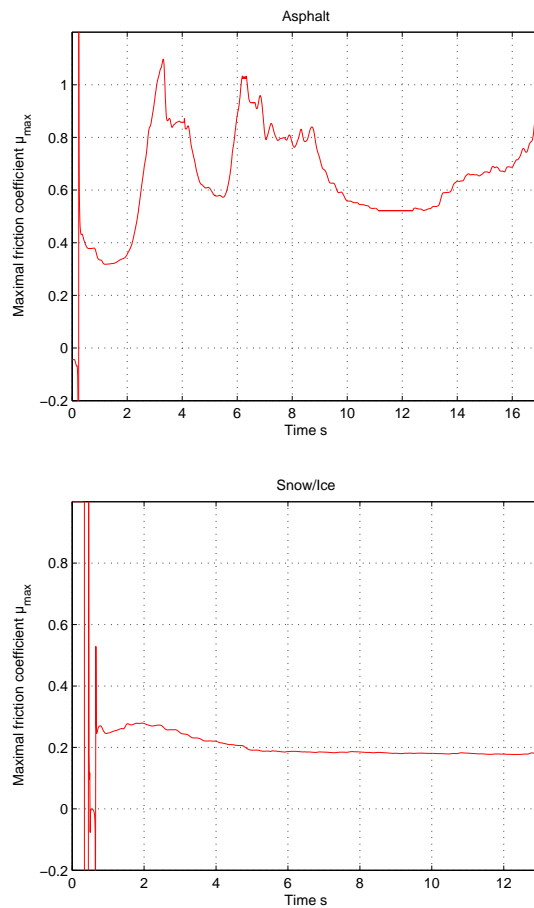


Figure 3.5: The plots shows the estimation of μ_{max} while softly accelerating on asphalt and snow/ice, respectively.

The estimation was done with a RLS-filter with forgetting factor. The RLS-filter

is given by the equations

$$\hat{\theta}_k = \hat{\theta}_{k-1} + P_k \varphi_k \epsilon_k \quad (3.20)$$

$$\epsilon_k = y_k - \varphi_k^T \hat{\theta}_{k-1} \quad (3.21)$$

$$P_k = \frac{1}{\lambda} \left(P_{k-1} - \frac{P_{k-1} \varphi_k \varphi_k^T P_{k-1}}{\lambda + \varphi_k^T P_{k-1} \varphi_k} \right) \quad (3.22)$$

and the forgetting factor λ is a number between 0 and 1. The trade-off is noise sensitivity versus parameter tracking speed. A large λ generates good noise suppression but a slow estimation. The RLS filter is easier to tune than the Kalman filter (only one tuning parameter) and since all three elements in the parameter vector should be estimated with equal accuracy, the RLS filter is a suitable choice of estimation algorithm. A thorough review of the RLS filter can be found in [19].

Chapter 4

Conclusions

In this chapter the two friction estimation approaches and the corresponding estimation results are discussed. Some thoughts concerning future work and possible improvements of the algorithms are also mentioned. Finally, the results when combining the vehicle dynamic control algorithm with the slip-slope based friction estimator are presented.

4.1 Slip-Slope Based Friction Estimation

Friction estimation, during normal driving, with the slip-slope based approach, seems to work quite good. The magnitude of the k -value is clearly different for different types of road surfaces. A distinction between a high friction (asphalt) and a low friction (snow/ice/skid pad) surface is definitely possible. With the gravel/rough road detector running in parallel with the slip-slope estimator also an intermediate friction level can be classified. Measurements and test drives also showed that the detection time when driving from a high to a low friction surface is no more than approximately 1-2 seconds. A gravel/rough road is detected in less than half a second. Since a change in friction can not be detected unless there is a change in slip (constant traction force effort and change in slip generates a change in the k -value) not all surface transitions are noticed within a few seconds. Test drives revealed that when the vehicle entered a low friction surface with very low engine speed (high gear) the change in slip was not large enough to result in a change in estimated slip-slope. In theory there is always a change in slip when driving from one surface to another but since the wheel speed measurements are rather noisy, the reality is a different thing. During the test drives it turned out that the above problem is solved by regularly changing the position of the gas pedal. That will lead to a direct change in traction force effort.

The main problem to overcome is to keep the estimated friction value stable during harder maneuvers. For example, sharp sinus turns (turning the steering wheel back and forth between -90 and 90 degrees) will affect the front wheel speed measurements and therefore such turns, on asphalt, can falsely be classified as gravel. Further, it is a quite tricky problem to choose a k -value threshold

for distinction between high and low friction. This is because of the fact that the k -value changes with a lot of factors, such as tire pressure and tire condition. Future work would be to identify the noise frequencies for the different sensors involved in the estimation process. Better and more sophisticated signal filters could then be used. The main signal problem now is the wheel speed measurements and the fact that the slip calculation amplifies the wheel speed noise. A better mapping of the k -value to friction is also needed. An inclusion of a similar estimation algorithm that can estimate the friction during braking would greatly increase the system availability.

4.2 Brush Model Based Friction Estimation

In theory the brush model can be used for direct estimation of the road-tire friction. The friction coefficient is explicitly included in the model and that makes it very suitable for different parameter estimation algorithms. As shown in Section 3.3, the brush model has high potential and when the input data are good the estimated friction value is rather accurate. But, as mentioned, the input data are seldom good during normal driving. That drawback resulted in that the estimated friction value was very hard to keep stable during test drives longer than approximately 15 seconds. Hence, the algorithm behavior during abrupt friction changes was hard to investigate. Another problem with the estimation algorithm used in Section 3.3 is that it can only deal with strictly positive slip and traction force effort values. A sign change in any of the inputs results in lost tracking of the friction value. Though, that problem can probably be solved by investigating algorithmic details. As for the slip-slope based estimation, the brush model based would perform a lot better with better filtered input data.

4.3 Vehicle Dynamic Control with Friction Estimation

The main goal with this thesis was to develop an algorithm that could estimate the road-tire friction coefficient online. As shown, that can be fairly accurately accomplished with the method based on slip-slope estimation. The additional goal was then to integrate the estimation algorithm within a vehicle dynamic control algorithm. As shown in Section 1.2, the behavior of the VDC algorithm can be made more dynamic and improved with knowledge of the current road-tire friction coefficient.

Investigations of the real influence of friction knowledge required a lot of test drives, which were performed at Bosch's test track in Boxberg. In one type of tests, the vehicle was driven from dry asphalt ($\mu_{max} \approx 0.9$) onto wet cobblestone ($\mu_{max} \approx 0.15$). During the test drives a typical output from the friction estimation algorithm looked like the plot in Figure 4.1. The algorithm successfully detects the abrupt road-tire friction change and the μ_{max} value is lowered from 0.9 to 0.6 and then shifts between 0.6 and 0.15. The algorithm is tuned in such a way that it can distinguish between high ($\mu = 0.9$), low ($\mu = 0.15$) and

intermediate ($\mu = 0.6$) friction values. The reason why the estimated friction value repeatedly shifts between two levels comes from the fact that the cobblestone surface is very uneven. Despite the surface high slipperiness, the wet cobblestone can, by the estimation system, also be considered as a rough road (the gravel/rough road detector is a separate but parallel running algorithm).

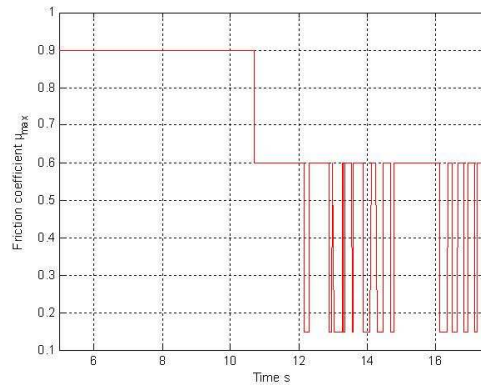


Figure 4.1: The figure shows the output from the friction estimation algorithm. The algorithm is tuned in such a way that it can distinguish between high ($\mu = 0.9$), low ($\mu = 0.15$) and intermediate ($\mu = 0.6$) friction levels.

On the low friction surface a few sinus turns were done in order to put the vehicle in a critical driving situation. A critical driving situation (unstability) is, as mentioned in Section 1.2, achieved when the force working on one of the axles (in this case the front axle) becomes larger than the maximum road-tire grip force (the friction circle boundary). The axle force and the maximum road-tire grip force is shown in Figure 4.2. As seen and in line with Section 1.2, the friction circle becomes smaller with decreasing road-tire friction coefficient. The front axle force is almost constant until the sinus turns begins and then correctly and quickly increases.

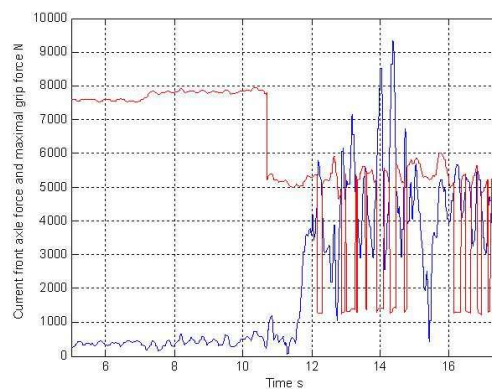


Figure 4.2: The red curve is the maximum grip force (or the friction circle boundary) and the blue curve the force working on the front axle.

During the time intervals where the axle force is larger than the friction circle

boundary the vehicle is said to be unstable and the VDC algorithm is taken into account. Figure 4.3 shows the time slots when the AFS system uses the output from the VDC algorithm. By comparing Figure 4.2 and 4.3 it is seen that the system works as intended and the VDC algorithm helps stabilizing the vehicle.

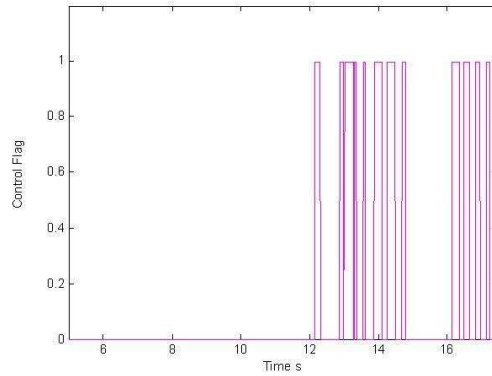


Figure 4.3: The figure shows the time slots when the VDC control signal is used by the AFS system.

It is clear that road-tire friction estimation improves the VDC algorithm. If the VDC algorithm, during the test drives, instead would have used the static criterion (1.1) (tuned for a high friction surface) the critical driving situation probably would have been noticed too late or perhaps not at all. With knowledge of the current road-tire friction coefficient also other VDC algorithm improvements can be made. One approach that gave a promising result was dynamic saturation levels of the desired road wheel angle. On a high friction surface the maximum desired road wheel angle should preferably be kept smaller than the same angle on a low friction surface. In further development of the algorithm, another interesting approach would be to test the effects of dynamic controller parameters. A type of friction coefficient depending gain scheduling.

Bibliography

- [1] P. Brosche. Modellbasierte regelung der quer- und gierdynamik eines fahrzeugs anhand automatischer lenkeingriffe der aktivlenkung. Diplomarbeit, Kassel University, Kassel, Germany, 2005.
- [2] J. Y. Wong. *Theory of Ground Vehicles*. John Wiley & Sons, Ltd, New York, NY, third edition, 2001.
- [3] T. D. Gillespie. *Fundamentals of Vehicle Dynamics*. Society of Automotive Engineers, Inc., Warrendale, PA, 1992.
- [4] C.-S. Liu and H. Peng. Road friction coefficient estimation for vehicle path prediction. *Vehicle System Dynamics*, 25:413–425, 1996.
- [5] S. Yamazaki, O. Furukawa, and T. Suzuki. Study on real time estimation of tire to road friction. *Vehicle System Dynamics*, 27, 1997.
- [6] L. Ray. Nonlinear tire force estimation and road friction identification: Simulation and experiments. *Automatica*, 33(10):1819–1833, 1997.
- [7] C. Canudas de Wit, P. Tsiotras, and X. Clayes. Friction tire/road modeling, estimation and optimal braking control. In *Lund NACO2 Workshop*, Lund, Sweden, 2001.
- [8] J.-O. Hahn, R. Rajamani, and L. Alexander. Gps-based real-time identification of tire-road friction coefficient. *IEEE Transactions on Control Systems Technology*, 10(3):331–343, May 2002.
- [9] F. Gustafsson. Slip-based tire-road friction estimation. *Automatica*, 33(6):1087–1099, 1997.
- [10] F. Gustafsson. Estimation and change detection of tire-road friction using the wheel slip. *IEEE Control System Magazine*, 18(4):42–49, 1998.
- [11] T. Dieckmann. Assessment of road grip by way of measured wheel variables. In *Proceedings of FISITA*, London, U.K., June 1992.
- [12] J. Svendenius. Tire models for use in braking applications. Licentiate thesis ISRN LUTFD2/TFRT–3232–SE, Department of Automatic Control, Lund Institute of Technology, Lund, Sweden, Nov. 2003.

- [13] J. Svendenius and B. Wittenmark. Review of wheel modeling and friction estimation. Technical Report ISRN LUTFD2/TFRT-7607-SE, Department of Automatic Control, Lund Institute of Technology, Lund, Sweden, Aug. 2003.
- [14] S. Muller and M. Uchanski. Slip-based tire-road friction estimation during braking. In *Proceedings of IMECE01*. ASME, 2001.
- [15] E. Ono, K. Asano, and M. Sugai. Estimation of automotive tire force characteristics using wheel velocity. In *IFAC Triennial World congress*, volume 15, 2002.
- [16] Vehicle dynamics terminology. SAE J670e, Society of Automotive Engineers, 1978.
- [17] E. Bakker, H. B. Pacejka, and L. Nyborg. Tyre modelling for use in vehicle dynamics studies. SAE Paper No. 870421, SAE, Warrendale, PA, 1987.
- [18] F. Gustafsson. *Adaptive Filtering and Change Detection*. John Wiley & Sons, Ltd, Chichester, U.K., 2000.
- [19] R. Johansson. *System Modeling and Identification*. Prentice Hall, Englewood Cliffs, NJ, second edition, Jan. 2004.
- [20] J. Gunnarsson. Recursive identification of time varying parameters. Master's thesis EX044/2001, Signalbehandling, Chalmers Tekniska Högskola, Göteborg, Sweden, Nov. 2001.
- [21] P. K. Nguyen and E. R. Case. The friction models and their effect on simulated vehicle dynamics. In *Proceedings of a Symposium on Commercial Vehicle Braking and Handling*, number UM-HSRI-PF-75-6, pages 245–312, 1975.

Appendix A

Derivations

A.1 Slip Computation During Cornering

While driving in a curve all four wheels have different angular velocities, hence the slip will not be the same for the left and right side. The curve radius R is defined as the distance from the curve center to the center of the rear axle. Since the prototype car is equipped with a yaw rate sensor the curve radius is easily computed from the relationship

$$R = \frac{v_x}{\dot{\psi}} \quad (\text{A.1})$$

where v_x is the vehicle's longitudinal velocity and $\dot{\psi}$ the yaw rate. The different curve radii, defined as the distances from the curve center to the driven wheels (see Figure A.1), are given by

$$\begin{aligned} R_{rl} &= R - L/2 \\ R_{rr} &= R + L/2. \end{aligned}$$

The choice of sign before $L/2$ depend on the fact that the yaw rate sensor signal is positive for left turns and negative for right turns. Since the vehicle's angular velocity around the curve center, the yaw rate, is a measurable value, the velocities of the driven wheels are obtained by

$$v_{rl} = \dot{\psi} R_{rl} = \dot{\psi} (R - L/2) \quad (\text{A.2})$$

$$v_{rr} = \dot{\psi} R_{rr} = \dot{\psi} (R + L/2). \quad (\text{A.3})$$

The cornering compensating slip computations now becomes

$$\hat{s}_{rl} = \frac{\omega_{rl} r_{rl}}{v_{rl}} - 1 = \frac{\omega_{rl} r_{rl}}{\dot{\psi} (R - L/2)} - 1 = \frac{\omega_{rl} r_{rl}}{v_x - \dot{\psi} \cdot L/2} - 1 \quad (\text{A.4})$$

$$\hat{s}_{rr} = \frac{\omega_{rr} r_{rr}}{v_{rr}} - 1 = \frac{\omega_{rr} r_{rr}}{\dot{\psi} (R + L/2)} - 1 = \frac{\omega_{rr} r_{rr}}{v_x + \dot{\psi} \cdot L/2} - 1. \quad (\text{A.5})$$

The cornering compensation just introduces a geometry correction term, so (2.16) and (2.17) still holds.

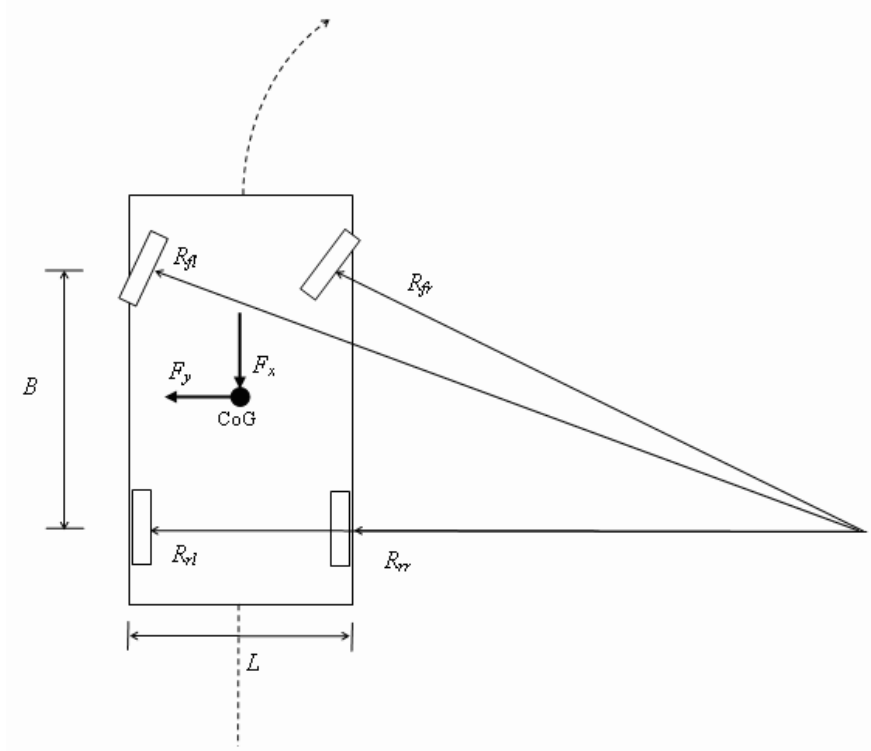


Figure A.1: The figure shows the different distances from the curve center to the the wheels while cornering.

A.2 Derivation of the Normal Forces

The normal forces acting on the two driven rear wheels are influenced by several different factors, which of some are difficult to model accurately. When the vehicle is standing still on level ground, the load on the rear axle depend only on the mass of the vehicle and the position of the center of gravity and with notation as in Figure A.2 that is

$$N_r = \frac{Mg \cdot b}{B}. \quad (\text{A.6})$$

During acceleration, load is transferred from the front axle to the rear axle. The acceleration force, F_x , is applied at the center of gravity and computed from Newton's second law

$$F_x = M \cdot a_x = M \cdot \frac{dv_x}{dt} = M \cdot \dot{v}_x. \quad (\text{A.7})$$

The contribution of the acceleration force depend on the ratio of height of CoG, h , to the wheelbase. The height of the CoG is assumed to be about equal to the height of the vehicle's engine's location. An additional force that influence the axle load during driving is the aerodynamic drag, F_a . The drag can be

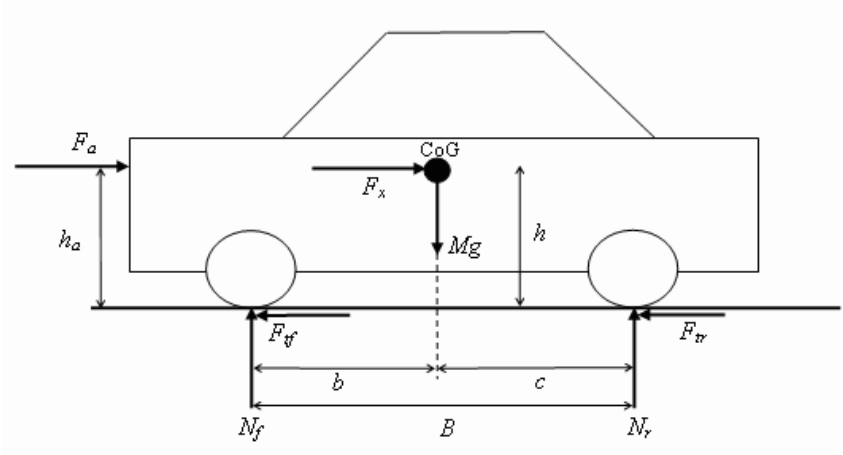


Figure A.2: The figure shows the different forces acting on the vehicle.

computed from the semi-empirical model

$$F_a = \frac{\rho c_d A v^2}{2} \quad (\text{A.8})$$

where

- ρ = Air density
- c_d = Aerodynamic drag coefficient
- A = Frontal area of the vehicle.

The air density is described by the equation

$$\rho = 1.225 \left(\frac{P_r}{101.325} \right) \left(\frac{288.16}{273.16 + T_r} \right) \quad (\text{A.9})$$

where

- P_r = Atmospheric pressure in kPa
- T_r = Air temperature in degrees Celsius.

The height of the aerodynamic force application, h_a , is approximated to be equal to h . The contribution of F_a depend on the same ratio as F_x . The rear axle load during straight driving then becomes

$$N_r = \frac{Mg \cdot b + h(F_x + F_a)}{B} \quad (\text{A.10})$$

During cornering the lateral acceleration forces must be accounted for. The lateral acceleration force is given by $F_y = \frac{mv^2}{R}$. But since the prototype car is equipped with a lateral acceleration sensor, the sensor signal multiplied with the vehicle's mass can be used instead (Newton's second law). The contribution to the normal force on the outer wheels is $F_y \frac{h}{L}$, where L is defined as in Figure

A.1. The normal force acting on each of the driven rear wheels can now be calculated as

$$N_{rl} = \frac{Mg \cdot b + h(F_x + F_a) - 2F_y \cdot \frac{h}{L} \cdot b}{2B} \quad (\text{A.11})$$

$$N_{rr} = \frac{Mg \cdot b + h(F_x + F_a) + 2F_y \cdot \frac{h}{L} \cdot b}{2B} \quad (\text{A.12})$$

The sign before the lateral force component depend on the actual sensor construction. A left turn generates a positive lateral acceleration and vice versa for a right turn. More detailed explanations and derivations can be found in [2] or [3].

